JOURNAL OF GUIDANCE, CONTROL, AND DYNAMICS
Vol. 23, No. 3, May–June 2000

Simulator Platform Motion Effects on Pilot-Induced Oscillation Prediction

Jeffery A. Schroeder
NASA Ames Research Center, Moffett Field, California 94035
and
William W. Y. Chung
Logicon Information Systems and Services, Moffett Field, California 94035

Simulator motion platform characteristics were examined to determine if the amount of motion affects pilot-induced oscillation prediction. Five test pilots evaluated how susceptible 18 different sets of pitch dynamics were to pilot-induced oscillations with three different levels of simulation motion platform displacement: large, small, and none. The pitch dynamics were those of a previous in-flight experiment, some of which elicited oscillations. These in-flight results served as truth data for the simulation. As such, the in-flight experiment was replicated as much as possible. Objective and subjective data were collected and analyzed. With large motion, pilot-induced oscillation and handling qualities ratings matched the flight data more closely than with small motion or no motion. Also, regardless of the aircraft dynamics, large motion increased pilot confidence in assigning handling qualities ratings, reduced safety pilot trips, and lowered touchdown velocities. Whereas both large and small motion provided a pitch rate cue of high fidelity, only large motion presented the pilot with a high fidelity vertical acceleration cue.

Nomenclature

a, b, c	= prefilter zeros and poles, rad/s
a_{model}	= model acceleration, ft/s^2, rad/s^2
a_{mot}	= motion system commanded acceleration, ft/s^2, rad/s^2
$F(x, y)$	= variance ratio with x and y degrees of freedom
$F_{\text{lon}}, F_{\text{lat}}, F_{\text{ped}}$	= longitudinal, lateral stick, and pedal force, lb
$\dot{h}_{\text{td}}$	= touchdown vertical velocity, ft/s
K	= control system prefilter gain
K_{mot}	= motion system filter high-frequency gain
K_θ	= control system gearing, deg/in.
$L_{\delta\text{lat}}$	= lateral control sensitivity, rad/s^2/in.
$M_{\delta e}$	= elevator control sensitivity, 1/s^2
$N_{\delta\text{lat}}$	= directional control sensitivity, rad/s^2/in.
n	= number of points in each mean
p	= probability that effects are random
s	= Laplace transform variable, rad/s
$T_{\theta 1}, T_{\theta 2}$	= pitch-to-elevator zero time constants, s
β	= sideslip angle, deg
δ_e	= elevator deflection, deg
δ_{ec}	= commanded elevator, deg
δ_{ecfilt}	= filtered commanded elevator, deg
δ_{estick}	= commanded elevator from stick, deg
$\delta_{\text{lon}}, \delta_{\text{lat}}, \delta_{\text{ped}}$	= longitudinal, lateral stick, and pedal deflection, in.
ζ_{dr}	= Dutch roll damping ratio
ζ_{mot}	= motion filter damping ratio
$\zeta_p, \zeta_{\text{sp}}$	= phugoid and short-period damping ratio
ζ_1, ζ_2	= control system prefilter damping ratios
ζ_ϕ	= numerator damping ratio in bank-to-aileron transfer function
θ, ϕ	= pitch and roll angles, deg

Jeffery Schroeder received a B.S. and M.S. from Purdue University and a Ph.D. from Stanford University in aeronautics and astronautics. Currently, he is the Deputy Chief of the Flight Control and Cockpit Integration Branch at NASA Ames Research Center, and he also serves as the part-time faculty at San Jose State University. His research interests include motion fidelity requirements, handling qualities, and pilot-vehicle-display design. He is an Associate Fellow of AIAA and a member of the AIAA Atmospheric Flight Mechanics Technical Committee. E-mail: jschroeder@mail.arc.nasa.gov.

William Chung received his B.S. degree in Industrial Engineering from Chung Yuan University, Taiwan, Republic of China, his M.S. degree in mechanical engineering from Oregon State University, and a second M.S. degree in aeronautics and astronautics from Stanford University. He is the Deputy Site Director at NASA Ames Research Center for Logicon Information Systems and Services. His primary research interest is in developing flight simulation fidelity requirements. He is a member of the AIAA Modeling and Simulation Technologies Technical Committee. E-mail: wychung@mail.arc.nasa.gov.

Received 29 June 1998; presented as Paper 98-4333 at the AIAA Atmospheric Flight Mechanics Conference, Boston, MA, 10–12 August 1998; revision received 13 September 1999; accepted for publication 15 September 1999.

τ_r, τ_s = roll and spiral mode time constants, s
ω_{dr} = Dutch roll natural frequency, rad/s
ω_{mot} = motion system filter natural frequency, rad/s
ω_p, ω_{sp} = phugoid and short-period natural frequency, rad/s
ω_1, ω_2 = control system prefilter natural frequencies, rad/s
ω_ϕ = complex zero natural frequency in bank-to-aileron transfer function, rad/s

Introduction

A PILOT-INDUCED oscillation (PIO) is "an inadvertent, sustained oscillation of the pilot-airframe system."[1] PIOs often escape detection in the aircraft design and development process, revealing themselves only during flight where the consequences can be catastrophic and costly, for example, the Shuttle, 777, C-17, YF-22, JAS-39, B-2, and V-22 (Ref. 2). Their causes are diverse, with some amenable to analysis[3–5] and some remaining intractable.[2]

Where analysis is incomplete, piloted simulation should be able to assist in detecting PIOs; however, its record is poor. Instead, simulators typically replicate and help fix PIOs that have occurred for the first time in flight. Recognizing this weakness, a recent study recommended that "validating simulation details, protocols, and tasks and collecting and correlating them with flight test results should be given high priority."[2]

Simulation can differ from flight in many ways, including inadequate vehicle models, poorer visual cues, imperfect motion cues, incomplete task demands, and lack of realistic stress. The U.S. Air Force started to examine the effect of these differences on PIO detection.[6] Two fixed-base simulators were compared using a previous flight test as the set of truth data.[7] For the in-flight configurations that were the most PIO prone, neither fixed-base simulator had strong correlation with flight.

The purpose of this study was to extend the previous effort by examining how the amount of simulator motion affects PIO predictability. Here, the same flight test was replicated with three simulator motion configurations: large motion, small motion, and no motion. Five pilots flew a landing task with 18 different sets of pitch dynamics with each motion configuration. Both objective and subjective data were recorded and compared with the previous flight test.[7] The experimental configuration is described first, followed by results, discussion, and conclusions.

Apparatus and Tests

Task

The NT-33 aircraft in-flight task was replicated as much as possible.[7] Pilots started at 135 kn and 1.5 n mile from the runway and flew three visual approaches to touchdown with each configuration. One approach was straight in, and one each started with a 150-ft left or right lateral offset from the touchdown point. During the approach, pilots were instructed to maintain constant speed and remain on the glidepath (−2.5 deg) and localizer. Deviations were indicated on head-down instruments. At the start of the run, the aircraft was placed $\frac{1}{2}$ dot off the desired localizer and glideslope.

For the left and right offsets, pilots held that offset until an automated voice instructed the pilot to correct. The pilot then maneuvered the aircraft to land on the desired touchdown point. The command to correct occurred when the runway overrun disappeared from the visual field of view, which corresponded to an altitude of 100 ft.

Figure 1 shows the desired touchdown point that was the near-left corner of the 1000-ft fixed distance marker located to the right of centerline. This desired touchdown point matched the flight-test study. Table 1 gives the performance standards for the task.

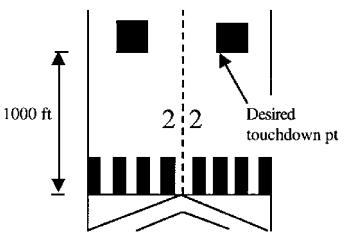

Fig. 1 Landing task.

Table 1 Task performance standards

Parameter	Desired	Adequate
PIOs	None	None
Longitudinal touchdown error, ft	±250	±500
Lateral touchdown error, ft	±5	±25
Approach airspeed, kn	±5	−5/+10

Table 2 Control system prefilters

Filter	K	a	b	c	ζ_1	ω_1	ζ_2	ω_2
B	3.0	3.3	10	——	——	——	——	——
D	0.5	20	10	——	——	——	——	——
1	1.0	——	——	——	——	——	——	——
2	10	——	——	10	——	——	——	——
3	4.0	——	——	4	——	——	——	——
5	1.0	——	——	1	——	——	——	——
6	16^2	——	——	——	0.7	16	——	——
7	12^2	——	——	——	0.7	12	——	——
8	9^2	——	——	——	0.7	9	——	——
9	6^2	——	——	——	0.7	6	——	——
10	4^2	——	——	——	0.7	4	——	——
11	16^4	——	——	——	0.93	16	0.38	16
12	2^2	——	——	——	0.7	2	——	——
13	3^2	——	——	——	0.7	3	——	——

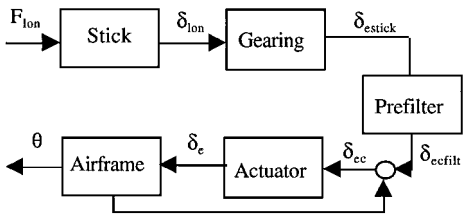

Fig. 2 Longitudinal block diagram.

Mathematical Model

Longitudinal Configurations

A linear stability derivative model[8] generated the aerodynamic forces and moments on the aircraft. Bare airframe derivatives were combined from several sources.[7,9,10] Response feedbacks of angle-of-attack and pitch rates to the elevator were used to simulate the different pitch configurations, given subsequently, that mimic the NT-33 variable stability aircraft.[9] Figure 2 shows a block diagram of the pitch axis dynamics.

The simulation centerstick dynamics were measured as

$$\frac{\delta_{lon}}{F_{lon}}(s) = \frac{0.125(22^2)}{s^2 + 2(0.7)(22)s + 22^2}$$

These dynamics are slightly slower than the 25-rad/s stick longitudinal natural frequency stated in Refs. 7 and 11 due to force-feel system limitations of this simulator cockpit. The ergonomics of the stick were matched to Ref. 11.

As in the flight experiment, 14 prefilters were simulated. These prefilters consisted of first-, second-, and fourth-order linear filters. Table 2 gives the values of these filters of the following form:

$$\frac{\delta_{ecfilt}}{\delta_{estick}}(s) = \frac{K(s+a)}{s+b}$$

$$\frac{\delta_{ecfilt}}{\delta_{estick}}(s) = \frac{K}{s+c}$$

$$\frac{\delta_{ecfilt}}{\delta_{estick}}(s) = \frac{K}{s^2 + 2\zeta_1\omega_1 s + \omega_1^2}$$

$$\frac{\delta_{ecfilt}}{\delta_{estick}}(s) = \frac{K}{\left(s^2 + 2\zeta_1\omega_1 s + \omega_1^2\right)\left(s^2 + 2\zeta_2\omega_2 s + \omega_2^2\right)}$$

Commanded elevator deflection was the sum of the prefilter output and the feedbacks of angle-of-attack and pitch rates. The elevator

Table 3 Aircraft dynamics

A/C	$T_{\theta 1}$	$T_{\theta 2}$	ζ_p	ω_p	ζ_{sp}	ω_{sp}
2	12	1.4	0.15	0.17	0.64	2.4
3	12	1.4	0.17	0.16	1.00	4.1
4	12	1.4	0.16	0.16	0.74	3.0
5	12	1.4	0.16	0.15	0.68	1.7

Table 4 Gearings

Configuration	K_θ	Configuration	K_θ
2-B	−2.94	3-8	−7.29
2-1	−2.94	3-12	−7.29
2-5	−4.33	3-13	−7.29
2-7	−2.94	4-1	−3.46
2-8	−2.94	4-2	−3.46
3-D	−8.65	5-1	−1.73
3-1	−7.29	5-9	−1.73
3-3	−7.29	5-10	−1.73
3-6	−7.29	5-11	−1.73

actuator was modeled using the following second-order filter with NT-33 actuator rate and position limits added[11]:

$$(\delta_e/\delta_{ec})(s) = 75^2/[s^2 + 2(0.7)(75)s + 75^2]$$

Four sets of aircraft dynamics were evaluated. The differences among the dynamics were effectively in the short-period mode. The pitch-to-elevator transfer function had the following form:

$$\frac{\theta}{\delta_e}(s) = \frac{M_{\delta_e}\left(s + 1/T_{\theta_1}\right)\left(s + 1/T_{\theta_2}\right)}{\left(s^2 + 2\zeta_p\omega_p s + \omega_p^2\right)\left(s^2 + 2\zeta_{sp}\omega_{sp}s + \omega_{sp}^2\right)}$$

Table 3 gives the parameters for the preceding transfer function. For all configurations, $M_{\delta e} = -3.3$ 1/s^2.

The remaining parameter to be specified is the gearing between the elevator command and the longitudinal stick position. For the 18 tested configurations, which represent combinations of the aircraft dynamics and prefilters, the gearings are listed in Table 4. As an example, for configuration 2-B, the 2 corresponds to the aircraft dynamics values in Table 3 and the B corresponds to the prefilter values in Table 2.

Subsequent to the experiment's start, information from the Ref. 6 authors indicated that the Table 4 gearings may have been 70% higher than in the flight test. To evaluate the effect of different gearings on the results, a miniexperiment was conducted using the Ref. 6 gearings with configurations 3-1, 3-D, and 3-12. Differences between gearings were less than or equal to one handling qualities and PIO point.

The 18 configurations were verified by performing frequency sweeps on each and overplotting the result against the frequency response of the analytical pitch-rate-to-stick-deflection transfer functions.

The engine model consisted of a first-order transfer function from throttle input to thrust output. The time constant was a nonlinear function of revolutions per minute (Ref. 11).

Lateral

By the use of a lateral-directional stability derivative model, coefficients were adjusted to achieve the following modal and sensitivity characteristics: $\tau_r = 0.3$ s, $\tau_s = 75$ s, $\omega_{dr} = \omega_\phi = 1.3$ rad/s, $\zeta_{dr} = \zeta_\phi = 0.2$, $|\phi/\beta|_{dr} = 1.5$, $L_{\delta_{at}} = 0.7$ rad/s^2/in., and $N_{\delta_{ped}} = -0.2$ rad/s^2/in. These characteristics were also verified with frequency sweeps.

Atmosphere

Dryden turbulence was used with rms magnitudes of 3 ft/s. A vertical 1-cosine gust occurred when the aircraft reached an altitude of 100 ft. The gust had a peak of 12 ft/s and was time scaled based on the 6.7-ft chord of the NT-33.

Safety Pilot

Evaluation pilots in the NT-33 flight study were accompanied by a safety pilot, who ended the evaluation and assumed control of the aircraft if a potentially hazardous situation occurred. If a safety pilot assumes control, then questions arise immediately on that configuration's controllability from the handling qualities point of view. The presence of a safety pilot can also add a factor of stress because another set of eyes is watching the evaluation pilot.

In this simulation, an automatic safety pilot was implemented that assumed control of the simulated model when the nosewheel's vertical speed exceeded −8 ft/s below a center-of-mass height of 12 ft. This criterion was developed empirically and was well received by the pilots. Upon activation, the pilot's cockpit controls went dead, a voice said "my airplane," and the mathematical model initiated a go-around.

Simulator

Motion System

The NASA Ames vertical motion simulator (VMS) was used.[12] It is the world's largest-displacement flight simulator with capabilities shown in Fig. 3. The cockpit was oriented for large longitudinal travel. The dynamics of the motion system were measured during the experiment using frequency-response testing techniques.[13] These dynamics were fit with an equivalent time delay in each axis. Software feedforward filters were used to tune the delays to achieve a close match among axes. The equivalent time delays for the surge, sway, pitch, roll, and yaw axes were all 80 ms, and the heave axis had 110 ms of delay. By comparison, delays in the NT-33 model following control system have been suggested as being in the 45–60 ms range.

Visual System

The visual scene was rendered with an Evans and Sutherland ESIG-3000 image generator. Three monitors comprised the field of view, as shown in Fig. 4. The visual system was tuned to have a

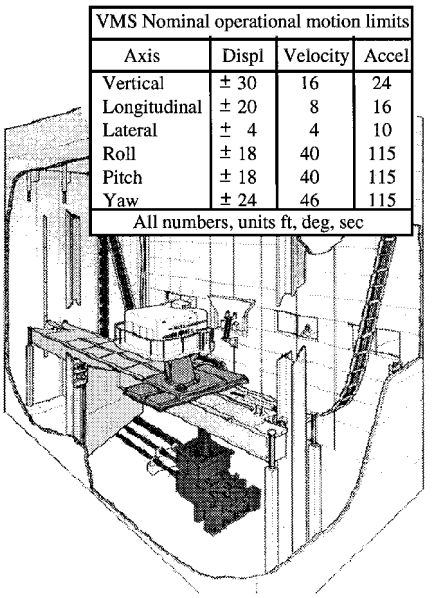

Fig. 3 NASA Ames Research Center vertical motion simulator.

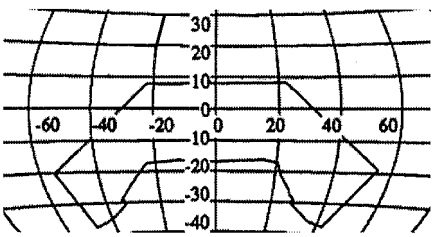

Fig. 4 Cockpit field of view.

Table 5 Large motion system parameters

Axis	K_{mot}	ω_{mot}
Pitch	1.00	0.20
Roll	0.40	0.50
Yaw	0.65	0.20
Longitudinal	0.65	0.40
Lateral	0.50	0.50
Vertical	0.80	0.30

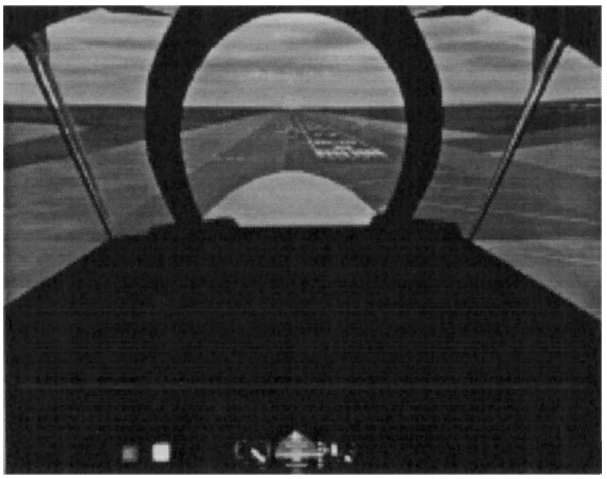

Fig. 5 Simulator cockpit photograph.

measured time delay of 80 ms from the pilot's stick position to the visual scene update, thus matching the equivalent motion delays in five axes. Figure 5 shows the visual scene with the aircraft near the runway. The nose of the simulated aircraft is at the bottom of the field of view. Window mullions were added (oval in Fig. 5) to replicate the cockpit as much as possible.[11]

Cockpit

The lateral stick and pedal dynamics were measured as

$$\frac{\delta_{lat}}{F_{lat}}(s) = \frac{0.25(16^2)}{s^2 + 2(0.7)(16)s + 16^2}$$

$$\frac{\delta_{ped}}{F_{ped}}(s) = \frac{0.0167(25^2)}{s^2 + 2(0.7)(25)s + 25^2}$$

A head-up display was video mixed with the visual scene. The display included a pitch ladder, altitude above sea level, airspeed, rate of climb, heading, range, and a flight-path marker. The flight-path marker represented center-of-mass flight path and used raw data only.

Motion Configurations

Three motion configurations were examined: large, small, and no motion. The VMS motion platform software was modified to implement each.

Large Motion

The classical washout motion control laws of the VMS were used for this configuration. Second-order high-pass (washout) filters exist between the mathematical model accelerations and the commanded motion system accelerations. These filters have the form

$$\frac{a_{mot}}{a_{model}}(s) = \frac{K_{mot}s^2}{s^2 + 2\zeta_{mot}\omega_{mot}s + \omega_{mot}^2}$$

In each of the six motion degrees of freedom, both K_{mot} and ω_{mot} were adjusted to keep the motion system within its displacement limits using motion system fidelity criteria suggested initially by Sinacori[14] and revised and validated subsequently.[15] Table 5 shows the values used. The damping ratio ζ_{mot} was 0.7. In addition to these cues, pitch/surge coordination and residual tilt crossfeeds were present in the motion logic.[16]

Small Motion

A coordinated-adaptive algorithm, used on many of today's hexapods, was employed in the small-motion configuration.[17,18] This algorithm was used with a mathematical model of a hexapod platform with 60-in. stroke actuators. Thus, the stroke limiting that occurs when commanding several axes simultaneously was present. Euler angles and translational positions of the platform were back solved on line from the resulting (and potentially limited) actuator positions.[19] The Euler angles and positions were then used to drive the VMS platform.

Second-order high-pass filters were used in the translational axes, whereas the rotational axes used a first-order high-pass filter (unlike the large-motion configuration). The second-order filters had a damping ratio of 0.7, except for the surge axis, which was 0.8. For comparison, Table 6 gives the gains and natural frequencies (or pole locations) for the small-motion filters. The gains listed are the maximum values because the coordinated-adaptive algorithm reduces these values when the actuators near their travel limits. These gains were adjusted to use as much of the 60-in. actuator stroke as possible.

No Motion

The motion system was turned off in this configuration.

Comparison with Fidelity Criteria

Figure 6 plots each axis of the large- and small-motion configurations against the validated criteria of Ref. 15. These points are determined by finding the magnitude and phase of the respective motion filter evaluated at 1 rad/s.

In the rotational axes, high motion fidelity is predicted for both pitch and yaw motion with the large- and small-motion configurations. Roll motion is low fidelity in both motion configurations because the roll axis was attenuated to minimize the false lateral specific force cuing during coordinated rolling maneuvers.

Table 6 Small-motion system parameters

Axis	K_{mot}	ω_{mot} (or pole)
Pitch	0.50	0.30 (pole)
Roll	0.25	0.81 (pole)
Yaw	0.70	0.30 (pole)
Longitudinal	0.11	0.67
Lateral	0.45	0.90
Vertical	0.13	0.90

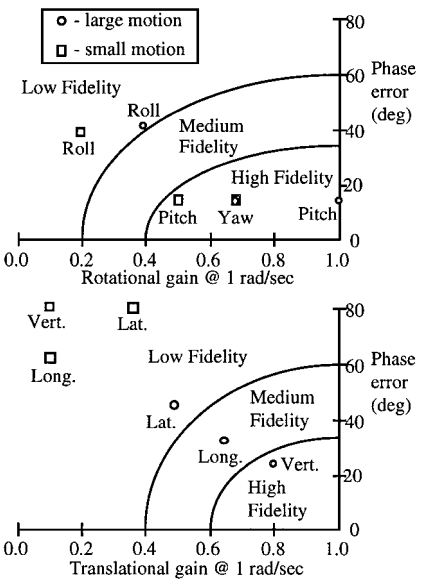

Fig. 6 Motion fidelity prediction.

In the translational axes, all of the small-motion cues are predicted to be low fidelity. For large motion, the fidelity improves, especially for the vertical axis, which provides a key cue for this task. Figure 6 shows the fidelity benefits of large motion.

Pilots

Five experience test pilots, hereafter referred to as A–E, participated. Pilot A was a Federal Aviation Administration test pilot, pilots B–D were NASA Ames Research Center test pilots, and pilot E was a Boeing Company test pilot.

Experimental Procedure

The experimental variables were 1) motion configuration (3) and 2) aircraft configuration (18). Thus, each pilot evaluated 54 configurations. Pilots A, B, and E evaluated each configuration at least twice. Pilots C and D evaluated each configuration once.

The pilots each read the same experimental briefing. They had no knowledge of the configurations, which were randomized. After flying the task, the pilots were told of their performance. Then, they assigned a handling qualities rating using the Cooper–Harper scale,[20] a pilot confidence factor,[20] and a PIO rating (PIOR).[10]

Results and Discussion

Objective Data

Example PIO

Figure 7 illustrates a classic divergent PIO that occurred with pilot B, configuration 3-12, and large motion. The pilot was nearly on the longitudinal stick stops. The pilot gave this configuration a Cooper–Harper rating of 8 and a PIOR of 5. PIOs of this severity and for this extended period of time did not occur for either the small- or no-motion configurations.

The average frequency of the PIO in Fig. 7 is 3.0 rad/s (the average in-flight PIO frequency of this configuration was 2.2 rad/s). Also shown on the pitch rate and normal acceleration traces are the motions that both the large- and small-motion configurations would produce for this visual motion.

At the PIO frequency, the large-motion configuration provides 100% of the pitch rate cue, and it leads the visual scene by only 5 deg of phase angle. Thus, the dashed line overlays the solid line. These values may be determined by inserting 3 rad/s into the motion system filter discussed earlier with the pitch axis parameters (Table 5). The small-motion configuration provided, at best, 50% of the visual pitch rate and leads the visual by 6 deg. By motion cuing fidelity standards, both the large- and small-motion cues are high fidelity.[14,15]

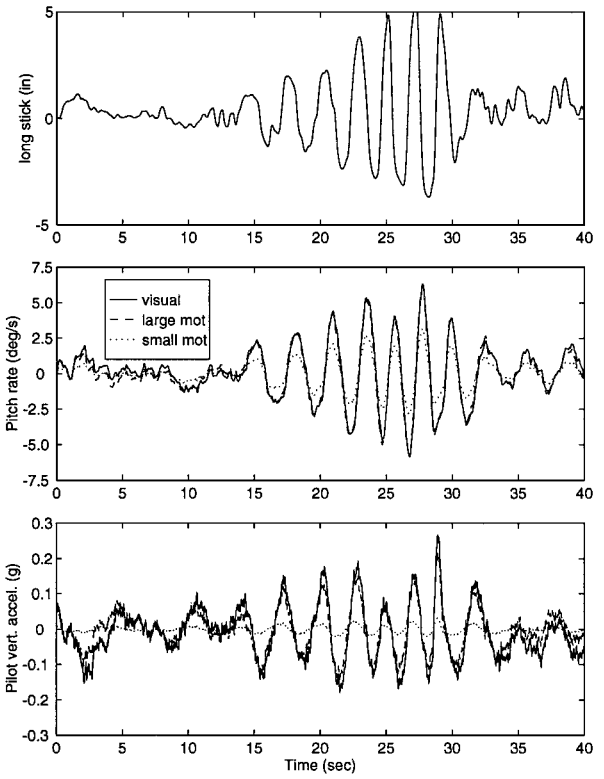

Fig. 7 Example PIO.

For the normal acceleration, the large-motion configuration provides 80% of the visual cue and leads the visual by 3 deg (this value includes the motion filter and the additional 30 ms of delay that the vertical platform lags the visual). However, the small-motion configuration provides only 13% of the visual cue and leads the visual by 20 deg. By motion cueing fidelity standards, the large-motion cue would be high fidelity, and the small motion cue would be low fidelity. It is for this important acceleration cue that large motion provides a simulation benefit, and it is likely the reason or the superior performance of the large-motion configuration, as discussed later.

Landing Performance

Longitudinal touchdown position was analyzed using a two-way repeated measures analysis of variance (ANOVA).[21] Whereas statistically significant differences occurred across the aircraft configurations [$F(17, 68) = 3.73$, $p < 0.001$], differences among the motion configurations were not found ($p > 0.2$).

Lateral touchdown position was analyzed, and no significant differences were noted among the aircraft ($p > 0.4$) or motion configurations ($p > 0.4$). Approach airspeed errors were almost always within the desired performance standard.

During the evaluations, it was noticed that pilots had difficulty in judging sink rate during the flare-to-touchdown when less platform motion was presented. Indications of this were either harder landings or the safety pilot assuming control for the small- and no-motion configurations.

Figure 8 shows the means and standard deviations of vertical touchdown velocities for each motion configuration. Each mean is an average of 90 points (18 configurations × 5 pilots). The ANOVA on these data indicated that the motion configuration affected touchdown velocity independent of the vehicle configuration [$F(2, 8) = 36.8$, $p < 0.001$]. Aircraft configuration also affected touchdown velocity independent of motion configuration [$F(17, 68) = 2.93$, $p < 0.001$]. No interaction between the motion and vehicle configurations was present ($p > 0.3$). Thus, touchdown velocity could be modeled as independent functions of the motion and aircraft configurations:

$$\dot{h}_{td} = f(\text{motion}) + g(\text{aircraft})$$

As more motion was available, pilots were able to lower the touchdown velocity. A previous limited experiment with large motion also indicated this effect when the longitudinal handling qualities were poor[22]; however, the results here indicate that large motion allows lower touchdown velocities regardless of the configuration.

As Table 1 notes, sink rate at touchdown was not a performance parameter in this experiment, which was also the case in the Ref. 7 flight experiment. In flight, pilots are likely able to use the richness of the visual cues better to regulate touchdown velocity. In contrast, the Ref. 6 simulation experiment added a touchdown performance criterion of $\leq$4 ft/s for desired performance and $\leq$8 ft/s for adequate performance. Had that been the case here, it is expected that even larger differences among the motion configurations would have occurred. This is because when more platform motion was added, it compensated for sink rate perception deficiencies in the visual scene.

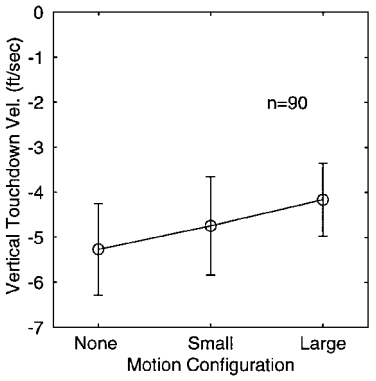

Fig. 8 Touchdown velocities.

Safety Pilot Trips

Figure 9 shows the number of times the automated safety pilot assumed control vs the motion configuration. Over 1400 landings were performed, and so the safety pilot assumed control in approximately 10% of the landings. It took control slightly fewer times with small motion than with no motion; however, large motion resulted in significantly fewer safety pilot trips. Many of the safety pilot trips occurred from the inability to judge sink rate.

Although it was stated earlier that having the safety pilot assume control should raise questions about the configuration's controllability, this seldom occurred because pilots often felt they were still in control of the vehicle. However, an alternative viewpoint is that the pilots could not control the sink rate to within a safe value if the safety pilot deemed a trip. Had this valid point been argued more strenuously by the authors, additional differences would likely have resulted among the motion configurations with the large-motion configuration performing even better.

Stick Activity

Longitudinal stick rms positions were analyzed. Statistical differences occurred across aircraft configurations [$F(17, 68) = 7.81$, $p < 0.001$], with configurations 5-10 and 3-12 having the most activity (0.96 and 0.93 in., respectively). Configurations 2-B and 3-D had the least activity (0.49 and 0.51 in., respectively). No significant differences occurred across the motion configurations ($p > 0.1$).

Handling Qualities Ratings

Large Motion

Figure 10 is a plot of the in-flight handling qualities ratings (HQRs)[7] vs the simulation HQRs for the large-motion condition. If simulation matched flight, then all points would lie on the diagonal line. A 1-unit HQR band is plotted about this line, which is often taken as the range of an acceptable match. Here 8 of the 18 configurations lie within this 1-unit band. Similar trends to that of the Ref. 6 fixed-based simulation are noted. That is, the best configurations in-flight were slightly worse in simulation, and the worst configurations in-flight were better in simulation.

Small Motion

Figure 11 shows the in-flight vs simulation HQRs for small motion. Here, 6 of the 18 configurations lie within the 1-unit band, which is a degradation from the large-motion condition. Again, the same trend on the best and worst configurations existed as for large motion.

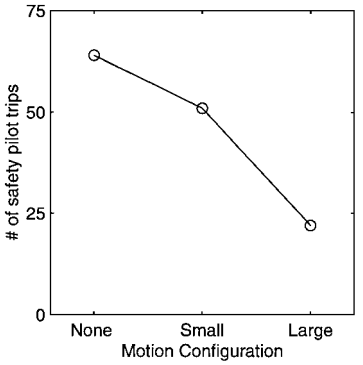

Fig. 9 Safety pilot trips.

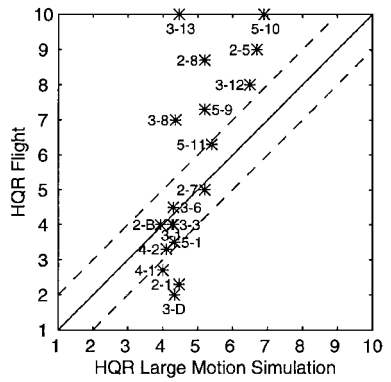

Fig. 10 Flight vs large-motion HQRs.

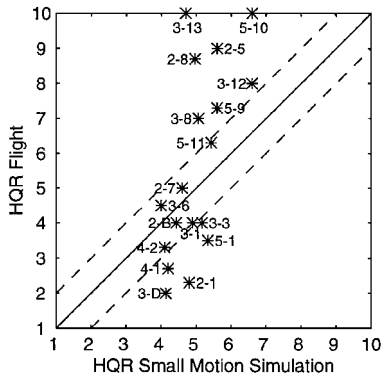

Fig. 11 Flight vs small-motion HQRs.

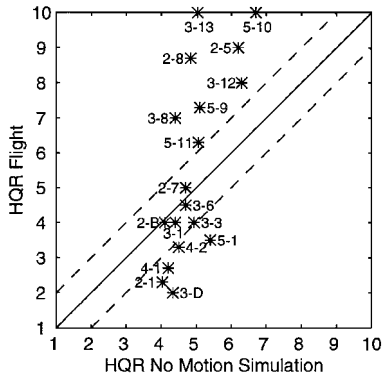

Fig. 12 Flight vs no-motion HQRs.

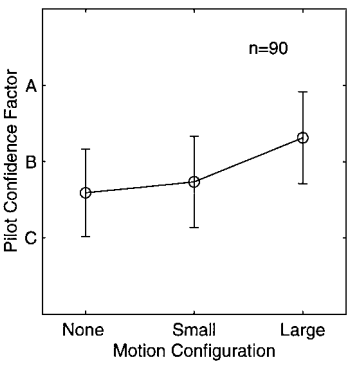

Fig. 13 Pilot confidence factors.

No Motion

Figure 12 shows the in-flight vs simulation HQRs for no motion. Here, 5 of the 18 configurations were within the 1-unit band, which is a degradation from large motion and small motion. Again, the same trend on the best and worst configurations existed as for large and small motion.

Pilot Confidence Factors

Confidence factors of A, B, and C refer to the pilots' opinion that they can assign an HQR with a high, moderate, or minimum degree of confidence, respectively.[20] Losses of confidence arise when simulation cues are incomplete or inadequate. Figure 13 shows that as more motion is provided, the pilot's confidence in assigning ratings improves. On average, both the no-motion and small-motion configurations caused the pilot to have less than a moderate degree of confidence in his rating. With large motion, that confidence improved to more than moderate. This difference was statistically significant across the motion configurations [$F(2, 8) = 5.82$, $p = 0.028$]. Differences in this measure were not significant across the aircraft configurations ($p > 0.1$).

PIORs

Large Motion

Figure 14 compares PIORs between flight and the large-motion simulation. Here 16 of the 18 configurations lie inside the ±1 PIOR

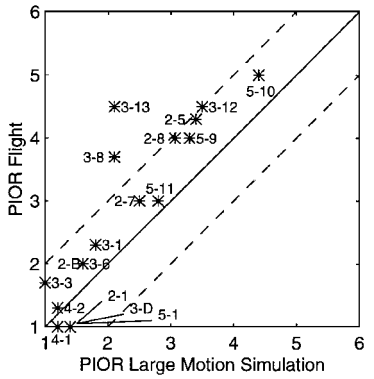

Fig. 14 Flight vs large-motion PIORs.

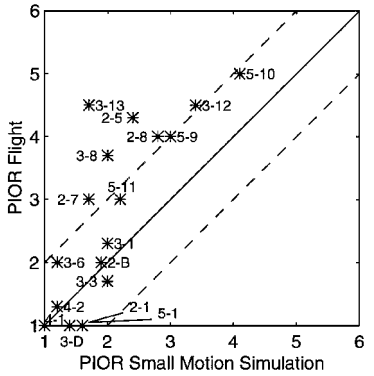

Fig. 15 Flight vs small-motion PIORs.

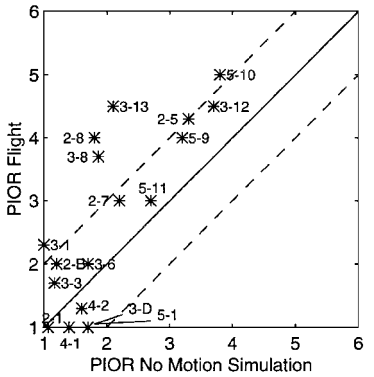

Fig. 16 Flight vs no-motion PIORs.

boundary. Except for four configurations, the in-flight PIORs were, on average, higher than the simulation PIORs.

Small Motion

PIORs for the small-motion configuration are shown in Fig. 15. Here, 12 configurations were inside the ±1 PIOR band, which was the worst performance of the motion configurations. Again, except for four configurations, the in-flight PIORs were worse than the simulator PIORs.

No Motion

The PIORs for no motion are given in Fig. 16. No motion performed slightly better than small motion, but worse than large motion. Here, 14 configurations were inside the ±1 PIOR band. Still, except for 4 configurations, the in-flight PIORs were higher than the no-motion PIORs.

Conclusions

A piloted experiment examined the differences among three levels of platform motion displacement in predicting PIOs. Objective and subjective measures were examined for large, small, and no platform motion. The small-motion condition represented the displacement of a conventional hexapod platform.

Overall, large motion matched flight more closely than either small or no motion. Specifically, large motion better matched the in-flight PIORs and the HQRs than did small or no motion. In addition, with large motion, pilots assigned higher confidence factor ratings, achieved lower touchdown velocities, and caused fewer safety pilot trips as compared to the other motion configurations. Finally, only with large motion did markedly divergent PIOs occur.

An example illustrated that high-fidelity pitch rate cues were provided by both the large- and small-motion configurations. However, only large motion allowed high-fidelity vertical acceleration cues to be presented. Pilots react strongly to vertical acceleration, and this likely contributed to the large-motion configuration providing the best results.

Acknowledgments

The authors thank Duc Tran, Soren Laforce, and Norman Bengford for the simulation software development and for their helpful suggestions on the experiment.

References

[1]Ashkenas, I. L., Jex, H. R., and McRuer, D. T., "Pilot Induced Oscillations: Their Causes and Analysis," Northrop-Norair Rept. NOR 64-143, Hawthorne, CA, June 1964.

[2]National Research Council Committee on the Effects of Aircraft–Pilot Coupling on Flight Safety, *Aviation Safety and Pilot Control—Understanding and Preventing Unfavorable Pilot–Vehicle Interactions*, National Academy Press, Washington, DC, 1997.

[3]McRuer, D. T., "Pilot-Induced Oscillations and Human Dynamic Behavior," NASA CR-4683, Dec. 1994.

[4]Klyde, D. H., McRuer, D. T., and Myers, T. T., "Unified Pilot-Induced Oscillation Theory Volume I: PIO Analysis with Linear and Nonlinear Effective Vehicle Characteristics, Including Rate Limiting," U.S. Air Force Research Lab., WL-TR-96-3028, Wright–Patterson AFB, OH, Dec. 1995.

[5]Bailey, R. E., and Bidlack, T. J., "Unified Pilot-Induced Oscillation Theory Volume IV: Time-Domain Neal-Smith Criterion," U.S. Air Force Research Lab., WL-TR-96-3031, Wright–Patterson AFB, OH, Dec. 1995.

[6]Kish, B. A., Leggett, D. B., Nguyen, B. T., Cord, T. J., and Slutz, G. J., "Concepts for Detecting Pilot-Induced Oscillation Using Manned Simulation," AIAA Paper 96-3431, Aug. 1996.

[7]Bjorkman, E. A., "Flight Test Evaluation of Techniques to Predict Pilot Induced Oscillations," Air Force Inst. of Technology, AFIT/GAE/AA/86J-1, Wright–Patterson AFB, OH, Dec. 1986.

[8]McRuer, D., Ashkenas, I., and Graham, D., *Aircraft Dynamics and Automatic Control*, Princeton Univ. Press, Princeton, NJ, 1973, pp. 203–295.

[9]Hall, G. W., and Huber, R. W., "System Description and Performance Data for the USAF/CAL Variable Stability T-33 Airplane," U.S. Air Force Flight Dynamics Lab., AFFDL-TR-70-71, Wright–Patterson AFB, OH, Aug. 1970.

[10]Smith, R. E., "Effects of Control System Dynamics on Fighter Approach and Landing Longitudinal Flying Qualities—Volume I," U.S. Air Force Flight Dynamics Lab., AFFDL-TR-78-122, Wright–Patterson AFB, OH, March 1978.

[11]Buethe, S. A., Govindaraj, K. S., and Knotts, L. H., "Description of NT-33A Configurations for Use in Programming NASA Vertical Motion Simulator (VMS)," Calspan Corp., Rept. 7205-5, Buffalo, NY, March 1984.

[12]Danek, G., "Vertical Motion Simulator Familiarization Guide," NASA TM 103923, May 1993.

[13]Tischler, M. B., and Cauffman, M. G., "Frequency-Response Method of Rotorcraft System Identification: Flight Applications to BO-105 Coupled Rotor/Fuselage Dynamics," *Journal of the American Helicopter Society*, Vol. 37, No. 3, 1992, pp. 3–17.

[14]Sinacori, J. B., "The Determination of Some Requirements for a Helicopter Flight Research Simulation Facility," NASA CR-152066, Sept. 1977.

[15]Schroeder, J. A., "Helicopter Flight Simulation Motion Requirements," NASA TP-1999-208766, July 1999.

[16]Rolfe, J. M., and Staples, K. J., *Flight Simulation*, Cambridge Univ. Press, Cambridge, England, U.K., 1986, pp. 116–120.

[17]Parrish, R. V., Dieudonne, J. E., Bowles, R. L., and Martin, D. J., Jr., "Coordinated Adaptive Washout for Motion Simulators," *Journal of Aircraft*, Vol. 12, No. 1, 1975, pp. 44–50.

[18]Martin, D. J., Jr., "A Digital Program for Motion Washout on Langley's Six-Degree-of-Freedom Motion Simulator," NASA CR 145219, July 1977.

[19]Dieudonne, J. E., Parrish, R. V., and Bardusch, R. E., "An Actuator Extension Transformation for a Motion Simulator and an Inverse Transformation Applying Newton–Raphson's Method," NASA TN D-7067, Nov. 1972.

[20]Cooper, G. E., and Harper, R. P., Jr., "The Use of Pilot Rating in the Evaluation of Aircraft Handling Qualities," NASA TN D-5153, April 1969.

[21]Myers, J. L., *Fundamentals of Experimental Design*, Allyn and Bacon, Boston, 1972, pp. 167–190.

[22]Bray, R. S., "A Study of Vertical Motion Requirements for Landing Simulation," *Human Factors*, Vol. 15, No. 6, 1973, pp. 561–568.